THE JOURNAL OF PHYSICAL CHEMISTRY C

Article

pubs.acs.org/JPCC

Large-Area Synthesis of Graphene on Palladium and Their Raman Spectroscopy

Xiaohong An,*[,†] Fangze Liu,[†] Yung Joon Jung,[‡] and Swastik Kar*[,†]

[†]Department of Physics and [‡]Department of Mechanical and Industrial Engineering, Northeastern University, Boston, Massachusetts 02115, United States

Supporting Information

ABSTRACT: We present a detailed investigation of the nucleation sites, growth, and morphology of large-area graphene samples synthesized via chemical vapor deposition (CVD) on bulk palladium substrates. The CVD chamber was systematically controlled over a large range of growth temperatures and durations, and the nature of graphene growth under these conditions was thoroughly investigated using a combination of scanning electron microscopy and a statistical analysis of >500 Raman spectra. Graphene growth was found to initiate at ∼825 °C, above which the growth rate increased rapidly. At T = 1000 °C, defect-free high-quality graphene was found to grow at an unprecedented rate of tens of micrometers per second, orders of magnitude faster than past reports on Cu- or Ni-based growth, thus leading to macroscopic coverage of the substrate within seconds of growth initiation. By arresting the growth at lower temperatures, we found that graphene nanoislands preferred to nucleate at very specific positions close to terrace edges and step inner edges. Evidence of both epitaxial and self-limiting growth was found. Along with monolayer graphene, both Bernal and turbostratic multilayer graphene could be obtained. A detailed evolution of the different types of graphene, as a function of both growth temperature and duration, has been presented. From these, optimal growth conditions for any chosen type of graphene sample can be inferred.

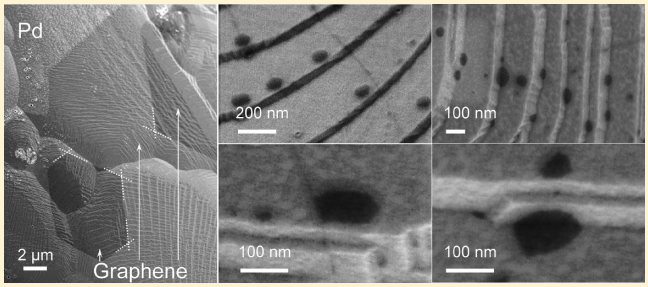

1. INTRODUCTION

In recent times, there has been explosive growth in the field of large-scale graphene synthesis[1] leading to an exciting new atomic-level understanding of C−C and C−substrate interactions at the fundamental level,[2−7] as well as their application developments in diverse fields such as nanoelectronics, optoelectronics, hybrid/composite materials, and energy-storage technologies.[8−14] In particular, due to its undeniable promise as a complementary metal-oxide semiconductor (CMOS) conformal material for next-generation two-dimensional (2D) electronic circuits and for the fabrication of large-area transparent conductive electrodes, the development of large-area graphene with low defect density and large crystallographic domains is in great demand. In this context, the chemical vapor deposition (CVD)-assisted growth of graphene on appropriate metal surfaces can be regarded as one of the most popular means of graphene production, due to its relative ease of synthesis, low cost of production of large-area high-quality graphene, and ease of transferability onto arbitrary surfaces for a host of advanced large-area applications, including photovoltaic panels[15] and touch-screen displays.[10]

Under appropriate growth conditions, both monolayered and multilayered graphene have been reported to grow on a number of different metal surfaces, including Cu, Co, Ni, Ir, Ru, Rh, Pt, Pd, etc.[16] Among these, CVD growth of graphene on Cu and Ni has received enormous attention for their low-cost scalability, and significant effort has been exercised to understand the nucleation, growth, and morphology of large-area graphene specimens on these substrates.[9,17−19] A large body of experiments has also explored a variety of fundamental aspects of the sp^2 carbon-growth kinetics on these and other metals, including the role of epitaxiality in graphene−substrate interactions, its resultant C−C bond formation energy, and the impact of various surface morphologies/defects.[20−24] A survey of literature reveals that despite the apparent ease with which graphene grows on a number of metals, the generic mechanism of large-scale sp^2 carbon formation on metallic surfaces is still an open topic due to the complex interplay between parameters such as the formation/nucleation energy, surface diffusion, and the solubility of C in the metal substrate under consideration. In addition, the underlying nature of the substrate at the nucleation sites (e.g., terraces, step edges, and grain boundaries) plays a significant role in altering the energy landscape of the substrate−graphene interaction. Due to its inherent importance in determining the size, shape, and morphology of the fully grown graphene sheets, a number of recent simulation works have also attempted to address the

Received: February 6, 2012
Revised: June 7, 2012
Published: July 12, 2012

dx.doi.org/10.1021/jp301196u | J. Phys. Chem. C 2012, 116, 16412−16420

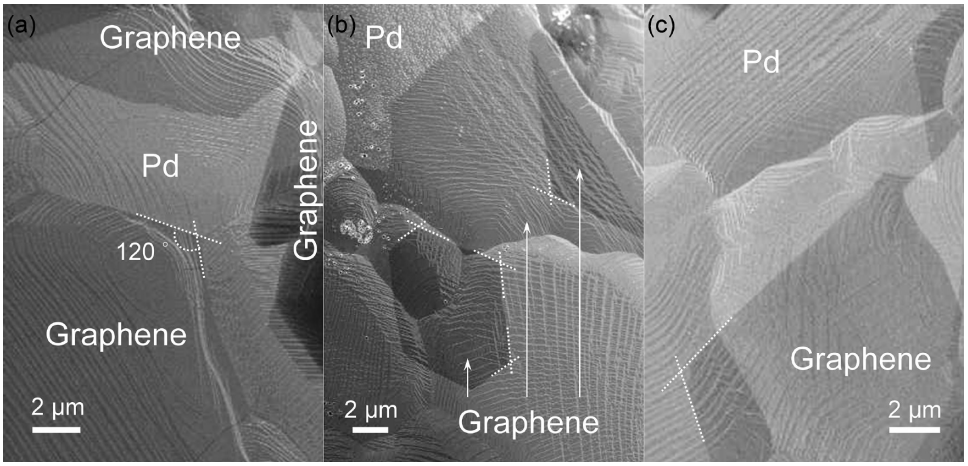

Figure 1. SEM images of CVD-grown graphene on Pd substrates (T = 1000 °C, t = 17 s), taken from representative regions of the substrate. The hexagonal-shaped graphene flakes and flake edges are seen to grow continuously over Pd terraces, step edges, and grain boundaries. The dashed lines demarcate 120° angles.

energetics of graphene nucleation and growth taking the above parameters into consideration.[21,25−30]

In this work, we present a detailed study of large-area growth of graphene on palladium substrates. As a noble transition metal, palladium has fascinated chemists for a variety of reasons, including its exceptional chemical stability and catalytic properties (including the catalytic cross-couplings in organic synthesis famously known as the Suzuki reactions),[31] and has been demonstrated to have important applications as catalytic converters and hydrogen-storage technologies. Palladium is also used in electronics, dentistry, medicine, hydrogen purification, chemical applications, and groundwater treatment.[32−35]A number of experimental works have explored the synthesis of Pd architectures on graphene.[36−38] However, despite extensive work on the growth of graphene on Ni and Pt (members of the same group as Pd) and a very early demonstration that graphene can be synthesized on palladium surfaces,[39] very little work has been done to explore the nature of large-area graphene synthesis on Pd substrates.

For a number of reasons, Pd is a unique substrate to explore graphene growth. Pd is a well-known "carbon sponge"[40] with a very well-studied carbon solubility and diffusivity.[41] The equilibrium C−Pd distance and binding energy per atom are different from those of the C−Pt and C−Ni systems,[42] which could potentially place it in a unique position within the elemental group. At typical growth conditions, Pd displays a rich variety of terrace structures allowing a possible investigation of a variety of growth-initiation conditions on the same metal. We have used a polycrystalline wire of palladium that also affords us a look at the effect of grain boundaries. Important from an application point of view, graphene grown on Pd appears to be semiconducting in nature,[43] with a band gap of ∼0.3 eV, and epitaxially grown graphene has orientation-dependent work function values.[44] Hence, both from a purely fundamental point of view and for suitable applications of these properties for device development, it is important to perform a systematic investigation of the nature of graphene growth on palladium substrates.

By arresting the growth at different stages through appropriate variations of the temperature and time intervals of growth and by investigating the growth at different regions of the metal substrate, we have been able to observe a number of important graphene growth characteristics on Pd surfaces. We have systematically explored the nature of the as-synthesized graphene through a combination of scanning electron microscopy and Raman spectroscopic analysis. We find that at temperatures of about 825 °C, hexagonal graphene islands ranging from a few to hundreds of nanometers in size appear to crystallize at preferential positions close to the ends of Pd terraces and step edges. At these temperatures, the growth is exceptionally slow (the island formation takes tens of minutes). Below these temperatures there is little or no evidence of graphene growth at all. With increasing growth temperatures, the growth rate increases rapidly, and at a growth temperature of ∼1000 °C, the entire macroscopic surface of the Pd wire gets covered within a few seconds and rapidly leads to the formation of multilayer graphene. The nature of the as-synthesized graphene is presented at different regions of growth and for different CVD running conditions that bring out the essence of the variety of growth mechanisms playing in this system. A detailed Raman analysis of the graphene enables us to identify different kinds of graphene, including monolayer, Bernal and turbostratic multilayer, and mixed Bernal−turbostratic graphene layers. We present a systematic study of the statistical evolution of various kinds of graphene as a function of temperature and growth duration. A combination of the SEM and Raman-statistical analysis enables us to establish for the first time the preferred nucleation sites of graphene on Pd substrates and the multiple growth mechanisms involved and provides a clear indication of conditions under which large-area single or few-layered graphene can be obtained.

2. EXPERIMENTAL SECTION

Graphene samples were synthesized by a low-pressure CVD growth technique[8] in a split tube furnace with a quartz tube (35 mm outer diameter). Pd substrates (Alfa Aesar, in the form of a 127 μm diameter wire, cut to a few millimeter long pieces) were placed in the center of the furnace with a flow of hydrogen (60 sccm) and argon (30 sccm). The whole system was kept under vacuum (1.5 Torr), heated to the growth temperature, and kept for 30 min in order to anneal the Pd wire and clean its surface of any unwanted oxide or physisorbed species before the growth of graphene. After that, methane gas (50 sccm) was introduced into the growth chamber for the growth of graphene at controlled intervals of time. During the growth process, the

dx.doi.org/10.1021/jp301196u | J. Phys. Chem. C 2012, 116, 16412−16420

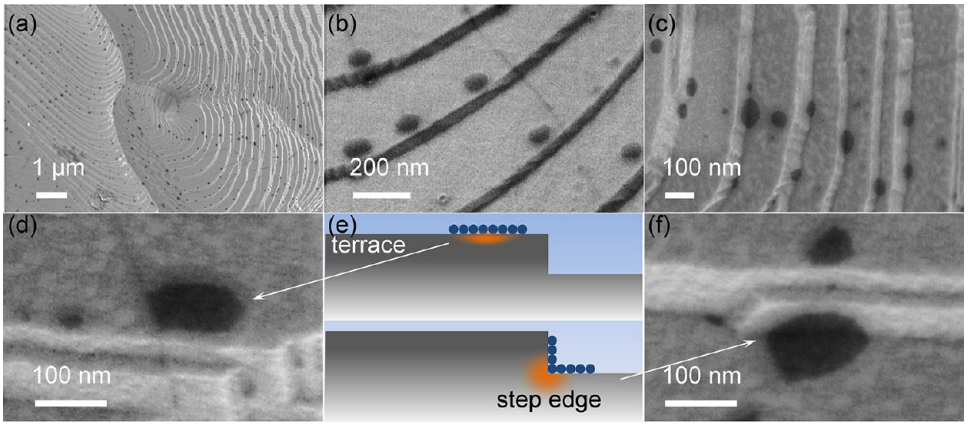

Figure 2. SEM images of arrested graphene growth on Pd substrates (T = 825 °C, t = 1800 s) taken from representative regions of the substrate. (a) Low-magnification image showing the uniform coverage of nucleation sites over the terraced Pd landscape. (b) Typical nucleation sites very close to the terrace edges. (c) Typical nucleation sites at the step inner edges. (d,f) High-magnification image of near-hexagonal graphene flakes (d) near a terrace edge and (f) at a step inner edge. A careful survey over large areas of the substrate reveals that most of the graphene flakes prefer to nucleate at either of these two energetically suitable sites, as highlighted schematically in (e) (not to scale).

vacuum of the whole system was kept at 2 Torr. Then, the furnace was allowed to naturally cool to room temperature under a pure argon flow. The synthesis of graphene on Pd wires was carried out at different temperatures (750, 800, 825, 830, 835, 840, 845, 850, and 1000 °C) for a fixed time interval of 30 min and for different time intervals (15, 16, 17, 25, 60, 180, 300, and 1800 s) at a fixed temperature of 1000 °C. In both cases, the time interval refers to the duration for which CH_4 was allowed to flow into the CVD chamber. The obtained graphene samples are characterized and analyzed by scanning electron microscopy (Zeiss Supra 25) and Raman spectrometry (Jobin Yvon LabRam HR800).

3. RESULTS AND DISCUSSION

At the highest growth temperature (i.e., at T = 1000 °C), there was little or no evidence of graphene growth for time intervals less than t_o = 15 s. For $t > t_o$, substantial coverage of the entire Pd substrate was obtained within seconds. Figure 1 is a collection of typical SEM images of well-formed graphene crystals on different regions of the Pd surface. From the shapes of the crystals, it is evident that they are polycrystalline, with single-crystal domains of a few to tens of micrometers in size. The edges of the graphene flakes form hexagonal shapes with ~120° edge angles and are found to grow continuously over multiple Pd grains across their grain boundaries. A closer inspection reveals that the surface of the Pd grains was heavily terraced with step edges, over which the graphene has grown continuously.

First principle studies of the shape of graphene edges under different growth conditions have shown that free-standing graphene flakes[28] with appropriate degrees of hydrogen edge-passivation can lead to hexagonally shaped single crystals. In the presence of substrates, the nature of the surface morphology of the metal substrate and its resultant carbon−substrate interaction can be expected to play a significant role in determining the flake shapes, size, and morphology. A number of recent works, which have explored the shape of growing graphene flakes,[2,6,7,23,24] have shown that graphene can grow both epitaxially (i.e., where the periodic arrangement of the hexagonal graphene surface maintains a constant relative alignment with respect to the crystal periodicity of the underlying substrate surface atoms) and nonepitaxially (i.e., graphene islands can continuously grow over regions of changing substrate orientations, such as across grain boundaries). In the former case, the orientation, shape, direction, and size of the graphene grains are usually limited by several factors, including the presence of step edges.[3,19,43] Even the shallowest of step edges (e.g., monatomic step edges) can restrict graphene growth. In the latter case, it has been shown that the graphene flakes can grow over substantially large areas and coalesce with neighboring flakes to form large polycrystalline films[2] with clear evidence of hexagonal edges. In this case, the surface morphology of metals appears to do little to restrict graphene growth, and the final shape/size is, hence, considered to be self-limited (i.e., could depend simply on the amount of C atoms supplied). In both cases, the first monolayer can form a template for epitaxial growth (i.e., the underlying graphene monolayer) of second or further layers. Under the growth conditions corresponding to Figure 1 (i.e., high temperature and very short growth time), the majority of the growth appears to be akin to the latter case (i.e., large-area, nonepitaxial, self-limited growth). Evidence of secondary epitaxial layers with edges oriented parallel to the primary template layer can be seen in Figure 1b. Most importantly, we find that at this growth temperature (T = 1000 °C), the growth was extremely fast (~10 μm/s) at 2 orders of magnitude faster than the CVD growth rate of graphene on both Cu and Ni substrates (several micrometers per minute) at comparable growth temperatures.[17]

Because of the rapid graphene growth (the entire surface was covered in a matter of seconds at T = 1000 °C), it was difficult to capture the initiation of graphene growth on Pd surfaces at higher temperatures. As the growth temperature was lowered, we found that there was a sharp cutoff, at approximately T_o = 825 °C, below which there was little or no graphene growth at all. At this temperature (which we refer to as the onset temperature), growth was extremely slow, and even large growth times (several tens of minutes) produced very small (10−100 nm) graphene islands located at extremely well-defined and preferential positions along the Pd surface. Figure 2 shows representative SEM images of graphene islands on Pd substrates obtained after a 30 min growth at T = 825 °C.

Figure 2a shows a low-magnification SEM image of the Pd surface, which is seen to be dotted with graphene islands all

dx.doi.org/10.1021/jp301196u | J. Phys. Chem. C 2012, 116, 16412−16420

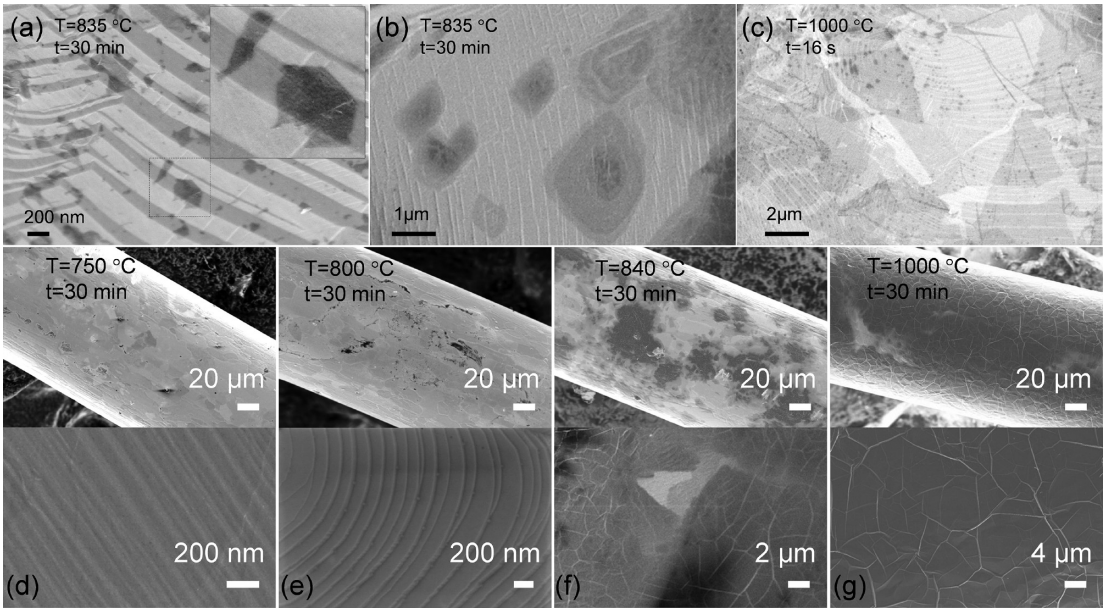

Figure 3. (a and b) SEM images showing two different modes of graphene growth (see text) just 10 °C above the onset temperature T_o = 825 °C. (c) SEM image showing large surface coverage with overlapping graphene flakes at T = 1000 °C, t = 16 s (growth begins at t_o = 15 s). (d–g) Typical coverage and morphology at two representative temperatures below the onset temperature and two above (growth time equals 30 min). The upper and lower panels represent low- and high-magnification images bringing out the coverage and morphologies, respectively. At these high-growth timescales, little or no growth is seen below the onset temperature and profuse amounts of graphitic carbon are seen above it.

over its terraced surface. Graphene nuclei are typically a few carbon atoms in size and, hence, impossible to discern using SEM even at the highest magnifications. Therefore, it was not possible to capture the shapes of graphene nuclei in these experiments. However, by arresting the growth to sub-100 nm flakes, we could easily infer the location of these nucleation sites. From Figure 2, a number of interesting features of the small graphene islands can be seen. High-magnification SEM imaging reveals that the graphene islands formed appear to have two preferred nucleation sites [i.e., either near the outer edge of (but not exactly at) a terrace, as seen in Figure 2 (panels b and d), or at the inner corner of a step edge, as seen in Figure 2c and f]. These observations were found to be almost ubiquitous across the entire polycrystalline Pd substrate. A number of theoretical models have studied the nature of graphene nucleation processes on terraces and step edges. These models have focused mainly on other transition-metal substrates as well as assumed monatomic steps, in most cases. In all cases, the energetics of graphene formation are related closely to the interplay of the local minima of formation energy and the edge energy of graphene nuclei. It appears that regions close to the front edge of a Pd terrace and the inner edge of a step are two energetically favorable locations for nucleation sites in Pd, possibly due to conducive strain–relaxed arrangements of the underlying Pd atoms at these locations. This has been schematically indicated by highlighting the corresponding regions of the substrate in Figure 2e. In addition to their chosen locations, the graphene islands also appeared to demonstrate an orientation preference with respect to the terrace/step structures. Wherever it was possible to visualize, it was found that the islands had an approximately hexagonal shape, with one of the edges parallel to the edge of the step, as seen in Figure 2d. This is a possible indication that under these lower-temperature conditions, the nucleation and growth of graphene are mostly epitaxial on the terraces and are most likely limited by surface structures of the underlying substrate. In addition, elongated hexagons were seen everywhere with their direction of elongation always parallel to the direction of the edge of the terrace indicating that this was a preferred direction of crystal growth due to a similar energy/strain consideration as discussed earlier.

Our experimental finding that graphene nuclei tend to form preferentially near the front edge of a terrace and not randomly anywhere on the terraces implies that a deeper analysis of the surface-strain relaxation and energetics of the underlying substrate[45,46] needs to be taken into consideration to understand realistic nucleation and growth of graphene at preferred locations. Similar considerations will be necessary for the inner step edges, where we find that graphene appears to grow equally well in both horizontal and vertical directions starting from the corner of the step edge. The controlled fabrication of nanostructured materials along steps and step edges is a field of great topical interest,[47,48] and indeed, these related observations in the graphene–Pd system could potentially lead to new degrees of control in methods for artificially engineering graphene nanostructures. We close the discussion on the nucleation sites by mentioning that on occasion, it was found that such sites were correlated with the positions of grain-boundary edges and triple points (see Supporting Information).

We next discuss how the graphene flake shapes evolve just after growth. As evident from Figure 2, at the onset temperature T_o = 825 °C, the size of the graphene islands are still small (~100 nm or less). As the growth temperature was increased, there was a sharp rise in the rate of graphene growth. Figure 3 (panels a and b) shows typical morphologies of graphene flakes on different regions of Pd substrate grown for 30 min at T = 835 °C. Two typical growth types were visible almost everywhere on the substrates. In the first case, graphene islands grew laterally "draping" over terraces and step edges, merging and coalescing as they grew. As seen in Figure 3a, this type of growth did not appear to maintain any isotropy

dx.doi.org/10.1021/jp301196u | J. Phys. Chem. C 2012, 116, 16412–16420

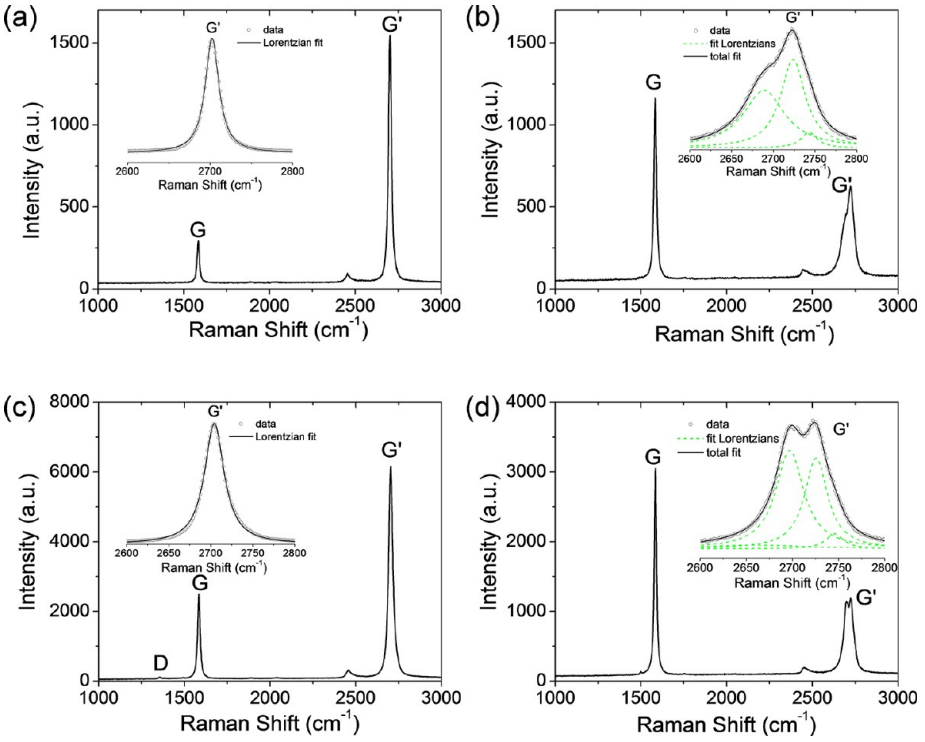

Figure 4. Typical Raman spectra of the four different categories of graphene samples found to grow on Pd (see text). (a) Monolayer graphene, (b) Bernal multilayer graphene, (c) turbostratic multilayer graphene, and (d) mixed species of graphene.

and, hence, was devoid of any regular geometric shapes. This indicates that while the nucleation and initial growth was epitaxial on a certain grain of Pd, the expansion beyond this grain continues in a self-limiting manner (nonepitaxial growth). The inset in Figure 3a shows an example of a flake that is beginning to lose its hexagonal shape and a second flake that does not have any regular shape at all. In comparison, a second growth mode was also found to occur under the same conditions, as seen in Figure 3b. In this mode, multiple layers of graphene grew epitaxially with respect to the first layer, and a regular geometrical shape was evident in these multilayer shapes even after they grew up to a few micrometers in size. Above these temperatures, the growth rate increased rapidly, resulting in the formation of large-area graphene samples possessing a variety of morphologies, which are discussed in detail below.

At the highest temperature (T = 1000 °C), little or no growth was found below an onset time interval of t_o = 15 s. The evolution of graphene growth with time was investigated at this temperature. Figure 3c shows the typical morphology of the graphene structures within 1 s of growth initiation (i.e., $t = t_o$ + 1 s = 16 s). As mentioned earlier, at this temperature graphene grows exceedingly fast, achieves a near-complete surface coverage, and further forms large overlapping layers. This overlapping phenomenon is rarely seen in graphene grown on Cu or Ni and leads to the formation of turbostratic multilayer graphene. It may be related to the high solubility limit of about 4% for carbon in Pd under 1000 °C, while the solubility limit of carbon in Pd under 825 °C is only 2%, which leads to the growth of small graphene islands. This is discussed in detail below.

Figure 3 (panels d–g) shows SEM images of representative areas of the Pd-wire substrates, with Figure 3 (panels d and e) representing growth temperatures below the onset temperature of T = 825 °C, and Figure 3 (panels f and g) showing two above it. For each case, the top and bottom panels are low- and high-magnification images, repsectively. In the higher-temperature cases, the surface of graphene is featured with "wrinkles" that are quite commonly observed in thick graphene layers as a result of strain relaxation. These panels demonstrate the absence of graphene below the onset temperature and a rapid coverage above the onset temperature. A detailed set of SEM images reflecting the nature of graphene samples as a function of growth duration have been placed in the Supporting Information.

A clearer picture of the evolution of graphene growth both as a function of temperature (for a fixed growth time of t = 30 min) and as a function of time (for a fixed growth temperature of T = 1000 °C) could be obtained by performing a comprehensive investigation of the graphene samples using Raman spectroscopy. Raman spectra were measured (excitation wavelength = 532 nm) for nine different growth temperatures and six different growth-duration values. In each case, 30–35 spectra were measured at approximately equal intervals of ~100 μm along the length of the Pd-wire substrates in order to obtain a representative statistical distribution for the different types of graphene samples. We have utilized these (>500 spectra) to classify the different types of graphene morphologies seen on the Pd surface. This sample size was found be adequate for a quantitative estimation of the different types of graphene samples observed on the Pd surface (discussed below), as we found that the data converged concurrently at the highest investigated growth temperatures and growth-time intervals.

Raman spectra of graphene have been studied extensively in the past.[49,50] The principal signature is a pronounced G band at ~1582 cm^{-1}, corresponding to the Raman active doubly degenerate zone center E_{2g} phonon (in-plane optical mode) of sp^2 hybridized carbon close to the Γ point. The D peak,

dx.doi.org/10.1021/jp301196u | J. Phys. Chem. C 2012, 116, 16412–16420

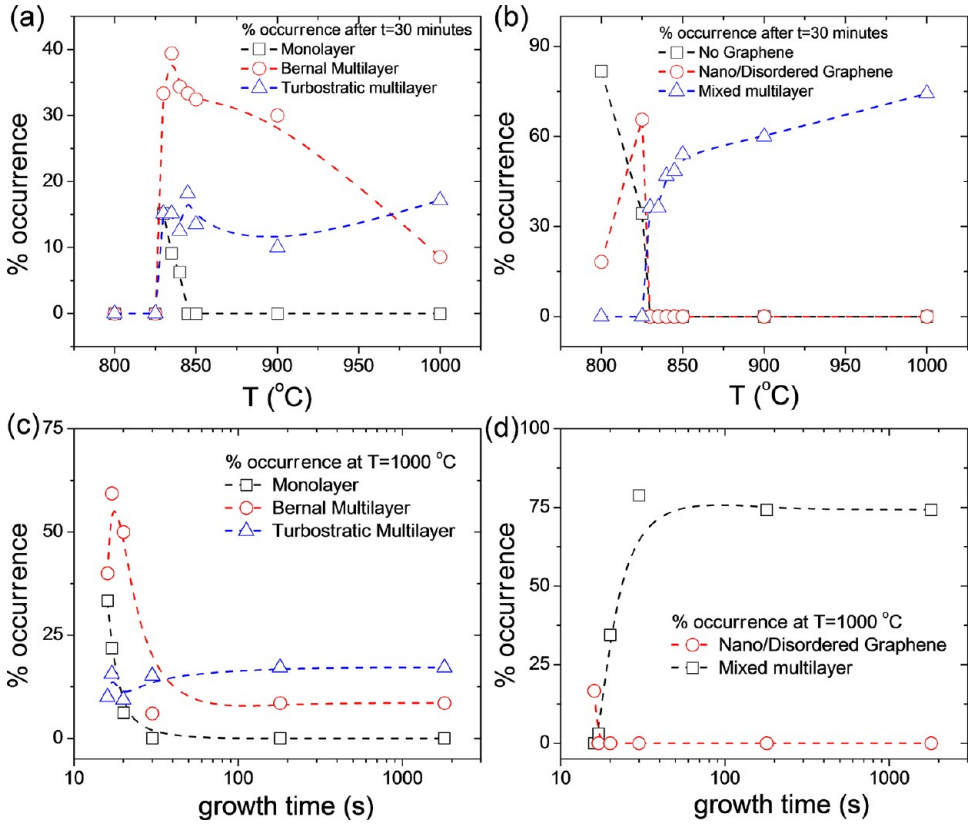

Figure 5. Evolution of the percentage occurrence of different categories of graphene on Pd substrates with (a and b) temperature and (c and d) time. These have been obtained from the categorization of the Raman spectra (see text).

observed at ~1350 cm^{-1}, corresponds to the first-order edge or defect-induced zone boundary phonons (absent in defect-free graphene and when the spectrum does not include signals from the edge of a flake). As seen in Figure 4, the D band was negligible or completely absent in all well-formed graphene samples, indicating the extremely high quality of graphene samples formed. One more informative signature, interchangeably termed as the 2D or the G′ peak/band, is usually located between 2600 and 2800 cm^{-1} and caused by the second-order zone boundary phonons. A careful analysis of the spectra reveals that our graphene samples could be broadly categorized into four different types.

The first type is that of monolayer graphene. These spectra featured the G peak at ~1583 cm^{-1} and a single-Lorentzian G′ peak around 2702 cm^{-1}, with a full width at half-maximum (fwhm) of ~20 cm^{-1} (less than 24 cm^{-1}).[49] Additionally, the relative intensities of the G′ peak to the G peak were found to be $I_{G'}/I_G > 5$, which are all signature characteristics of monolayer graphene. Figure 4a shows a typical Raman spectrum from a monolayer graphene sample, with an inset showing the single-Lorentzian fit to the G′ peak. The graphene samples seen in Figure 1 (panels a and c) are examples of regions from which such spectra could be obtained.

The second type of Raman spectra are those of multilayer graphene with Bernal (AB) layer stacking which have G peaks at roughly the same position as those of monolayer graphene. However, in these samples, the G′ peak splits into multiple (3−6) Lorentzians, depending on the number of layers of graphene under the laser spot.[49] Figure 4b shows a typical Raman spectrum of such a multilayer graphene. The inset shows the G′ band, which could be fitted using three Lorentzian peaks, indicating the presence of four-layer graphene. The overall intensities of the G′ peak of these spectra were found to be comparable or lower than those of the G peak, while the intensities of G peaks were higher than those of monolayer graphene (for the same incident laser power). These can be attributed to the increased number of graphene layers, which provide more signal in the Raman spectrum under consistent measuring conditions. Regions of Figures 1b and 3b where multiple layers are seen provided such Raman spectra. These properties of the peaks are consistent with past reports of Raman spectra of Bernal-stacked multilayer graphene.

In the third type, the Raman spectra look similar to that of monolayer graphene, even though visual inspection (i.e., using SEM or sometimes even an optical microscope) indicated the presence of multiple layers. Figure 3c shows a typical region where such spectra could be obtained, where randomly oriented overlapping layers of graphene were found, presumably due to neighboring nucleation sites that grow into large flakes that overlap each other. These spectra were attributed to the presence of turbostratic multilayer graphene.[49] Unlike Bernal-stacked graphene, the individual layers in turbostratic multilayer graphene do not possess any rotational coordination, and the interlayer separation in this type of multilayer graphene is about 0.3440 nm (larger than that of the Bernal case, which is 0.3354 nm). Figure 4c shows a typical Raman spectrum that shows a G peak at ~1584 cm^{-1} and a slightly blue-shifted G′ peak at 2704 cm^{-1}. The G′ peak could be fit with a single Lorentzian (see inset of Figure 4c), while the fwhm widens to ~28.4 cm^{-1} (recall that for monolayer graphene, fwhm < 24 cm^{-1}). In all these spectra, the G′ peaks were found to be larger than the G peaks, but the ratio $I_{G'}/I_G$ reduced to <2.5. In

dx.doi.org/10.1021/jp301196u | J. Phys. Chem. C 2012, 116, 16412−16420

addition, the intensities of the G peak were much higher than those of monolayer graphene (compare the example with Figure 4a) under the same incident laser power and other measuring conditions, consistent with the presence of multiple layers.

Finally, a number of spectra found do not conform to the above three types. They were invariably obtained at locations of thicker growth (e.g., regions seen in Figure 3f). Figure 4d shows such a spectrum. Although the G′ peak could be fitted with multiple Lorentzians (as seen in the inset of Figure 4d), they show no resemblance to known shapes for monolayer graphene, Bernal multilayer graphene, turbostratic multilayer graphene, or graphite.[50] Their intensities were usually stronger than those of Bernal or turbostratic multilayer graphene, consistent with the regions of thicker growth. In all likelihood, these spectra were obtained at regions where several types of graphene (two or more from types 1−3 mentioned earlier) formed layers under the laser spot. These spectra were clubbed together into the fourth category, which we call mixed multilayer graphene.

In addition to these four categories, in some cases Raman spectra are typically representative of nanoscale or disordered graphitic carbon. In the case of low growth temperatures, where the Pd samples were mostly covered with graphene nanoislands as seen in Figure 2, these spectra typically comprised a G peak accompanied by a clear D band (possibly a flake-edge effect) and, often, a weak G′ band. In other cases, where carbonaceous material covered the Pd surface without any long-range graphitic order, some signals of widely overlapping G and D bands were also seen. These spectra (not shown) were combined into a category that we call "nano/disordered graphene". All the aforementioned spectra were useful for obtaining a clearer picture of the evolution of graphene morphologies as a function of temperature and time.

Figure 5a shows the evolution of the percentage occurrence of monolayer, Bernal multilayer, and turbostratic multilayer graphene as a function of growth temperature (growth duration = 30 min). Growth commences at about T_o = 825 °C, following which there is a sharp rise in growth rate, both observations being consistent with the SEM investigations discussed earlier. Within a few tens of degrees Celsius, the surface of Pd is covered with all three types of graphene. Monolayer graphene covers about 15% at the maximum point, beyond which its occurrence was found to decrease. The percentage occurrence of turbostratic multilayers remains between 10 and 20%, reaching a value of about 17% at the highest investigated temperature of T = 1000 °C. These were likely an outcome of overlaps between expanding neighboring monolayer graphene flakes which do not stop growing at the flake edges but rather keep growing laterally by one climbing on top of the other as seen in Figure 3c.

Bernal multilayers were found to grow initially at a rate much higher than either of the other two types and were found to occur at 30−40% of the investigated locations up to a growth temperature of T = 850 °C. Beyond this temperature, there was a slow decline in their occurrence, and the surface was found to be occupied more frequently by the mixed multilayer type of graphene, as seen in Figure 5b. This is consistent with the fact that as the growth temperature was increased, there was an increased overlap between different types of multilayer graphene samples on the surface of Pd. However, despite the rapid growth of graphene at the highest temperatures, the surface of the Pd substrate was not found to be covered with only the mixed type, as seen from Figure 5 (panels a and b), indicating that beyond some critical thickness, the graphene layers do no prefer to overlap each other. This fact becomes clearer in the time-evolution study discussed next.

Figure 5c shows the percentage occurrence of monolayer, Bernal multilayer, and turbostratic multilayer graphene as a function of time (15 s < t < 2000 s) at the highest investigated growth temperature, T = 1000 °C. At this temperature, we found little or no evidence of graphene growth for time intervals less than t_o = 15 s. Past work on graphene growth on Cu and other substrates has shown that a critical surface concentration of C atoms is required before nucleation and growth occur.[21,29] We believe that this onset time interval of t_o = 15 s was required for an adequate amount of surface C species to be deposited from the source at T = 1000 °C. It is seen that beyond this timescale, which we call the nucleation time, growth is extremely rapid. By allowing the CH_4 to flow for selective time intervals ranging from a few seconds to 30 min, we were able to quantitatively observe the time evolution of the surface coverage (in terms of the percentage occurrence) of the different types of graphene growth independently using Raman spectroscopy. From Figure 5c, it is evident that within 1 s of the nucleation time (i.e., t = 16 s), about 35% of the investigated areas of the surface of the substrate was covered with monolayer graphene, while about 40% showed the presence of Bernal multilayer graphene. The occurrence of turbostratic multilayer graphene seemed to remain more or less a constant and saturated to a value of about 17% within a few tens of seconds after nucleation.

As seen in Figure 5c, the percentage occurrence of monolayer and Bernal multilayer graphene reaches a peak within the first couple of seconds after nucleation and then rapidly falls over the next tens of seconds, reaching values of 0% and about 9%, respectively, at the highest-growth time interval of t = 30 min. During these timescales, these species were replaced by the mixed multilayer graphene samples, as seen in Figure 5d. Within this same timesscale of a few tens of seconds, mixed multilayer graphene grows rapidly to occur at almost 74% of the investigated areas, matching nicely with its percentage occurrence in the higher end of the temperature-dependence graph (Figure 5b).

Figure 5 (panels c and d) brings out an extremely interesting feature of multilayer graphene growth on the Pd surface. It appears that by a relatively short timescale of t = 100 s, each of the different types of multilayer graphene samples produced on the surface of Pd reaches some kind of equilibrium and does not evolve further with time. Since each data point on these graphs represents measurements on separately grown samples, this is not some artifact of an individual piece of substrate. There appears to be some kind of an equilibrium distribution of the three kinds of graphene species which we do not yet understand clearly. It could be assumed that the initially grown monolayer species (that grows within a second of nucleation) rapidly decreases in percent occurrence due to their conversion into either a Bernal multilayer (possibly by the formation of subsequent layers in an epitaxial manner, as seen in Figures 1b and 3b) or a turbostratic multilayer as seen in Figure 3c. We believe that these observations could open pathways for a greater understanding of the dynamics of C species on Pd and would most likely benefit enormously from theoretical/computational modeling efforts. In addition, a systematic work on trying to understand the underlying mechanism for the stabilization of different types of graphene species on Pd

could possibly lead to development of methodologies for the controlled growth of graphene of different types for diverse application-specific requirements on this substrate.

4. CONCLUSIONS

To conclude, we have performed a detailed investigation of the nucleation, growth, and morphology of CVD-assisted large-area graphene growth on a relatively new substrate, palladium. Large-scale growth on palladium shows unique new features previously unreported on commonly used substrates such as Cu and Ni. By arresting the growth at different stages, we have shown that nucleation of graphene on Pd is preferred along specific positions of Pd terrace edges and step inner edges. Under well-controlled low-pressure CVD growth, well-defined onset temperatures and nucleation times have been identified, which could potentially provide key inputs to modeling efforts. At high temperatures, growth rates which are orders of magnitude higher than those of Cu and Ni were found. Detailed analysis of Raman spectroscopy enabled us to clearly identify the multiple growth mechanisms present in this system. It also helps us to quantify optimal growth conditions for high-rate monolayer growth. For example, rapid monolayer growth can be obtained at high temperatures and very short growth durations. A recent work[51] has shown that via control of the concentration gradient of the carbon source along the length of a CVD chamber, graphene samples of varying thicknesses can be grown on Cu substrates in a controllable manner. From this work, it appears that thicker graphene layers can arise when the mass transport of carrier gases becomes the dominant rate-determining mechanism (rather than the surface kinetics), and this could be an important factor in determining the layer thickness of graphene grown on Pd. Further, depending on the type of application, multilayer growth of different morphologies can also be controlled in a similar manner. We believe that this work opens the path for new levels of understanding in C–substrate interactions and their reaction kinetics, which is a key factor in large-area graphene growth, and will lead to a number of potential applications where high-rate production of graphene and advanced applications using graphene–Pd hybrid systems are envisioned.

■ ASSOCIATED CONTENT

Supporting Information

SEM images (Figure S1) of typical examples of graphene nucleation and growth at grain boundaries and other possible defect locations on Pd surfaces and SEM images (Figure S2) reflecting the evolution of graphene growth as a function of time at T = 1000 °C. This material is available free of charge via the Internet at http://pubs.acs.org.

■ AUTHOR INFORMATION

Corresponding Author

*X.A.: e-mail, x.an@neu.edu. S.K.: e-mail, s.kar@neu.edu.

Notes

The authors declare no competing financial interest.

■ ACKNOWLEDGMENTS

S.K. acknowledges the financial support provided by NSF ECCS 1102481, and Y.J.J. acknowledges partial support from the Fundamental R&D Program for Core Technology of Materials in the Ministry of Knowledge Economy, Republic of Korea. We also acknowledge the Global Frontier Research Center for Advanced Soft Electronics and Grant 2011-0017333 of the National Research Foundation of Korea for partial financial support.

■ REFERENCES

(1) Kar, S.; Talapatra, S. Synthesis of Graphene; Bhushan, B., Ed.; to appear in the *Encyclopedia of Nanotechnology*, DOI 10.1007/978-90-481-9751-4, Springer Science+Business Media B.V., 2012.
(2) Yu, Q.; Jauregui, L. A.; Wu, W.; Colby, R.; Tian, J.; Su, Z.; Cao, H.; Liu, Z.; Pandey, D.; Wei, D.; Chung, T.; Peng, P.; Guisinger, N. P.; Stach, E. A.; Bao, J.; Pei, S.; Chen, Y. P. *Nat. Mater.* **2011**, *10*, 443–449.
(3) Sutter, P. W.; Flege, J.; Sutter, E. A. *Nat. Mater.* **2008**, *7*, 406–411.
(4) Lahiri, J.; Lin, Y.; Bozkurt, P.; Oleynik, I. I.; Batzill, M. *Nat. Nanotechnol.* **2010**, *5*, 326–329.
(5) Coraux, J.; N'Diaye, A. T.; Busse, C.; Michely, T. *Nano Lett.* **2008**, *8*, 565–570.
(6) Wu, B.; Geng, D.; Guo, Y.; Huang, L.; Xue, Y.; Zheng, J.; Chen, J.; Yu, G.; Liu, Y.; Jiang, L.; Hu, W. *Adv. Mater. (Weinheim, Ger.)* **2011**, *23*, 3522–3525.
(7) Robertson, A. W.; Warner, J. H. *Nano Lett.* **2011**, *11*, 1182–1189.
(8) Li, X.; Cai, W.; An, J.; Kim, S.; Nah, J.; Yang, D.; Piner, R.; Velamakanni, A.; Jung, I.; Tutuc, E.; Banerjee, S. K.; Colombo, L.; Ruoff, R. S. *Science* **2009**, *324*, 1312–1314.
(9) Reina, A.; Jia, X.; Ho, J.; Nezich, D.; Son, H.; Bulovic, V.; Dresselhaus, M. S.; Kong, J. *Nano Lett.* **2009**, *9*, 30–35.
(10) Bae, S.; Kim, H.; Lee, Y.; Xu, X.; Park, J.; Zheng, Y.; Balakrishnan, J.; Lei, T.; Kim, H. R.; Song, I. Y.; Kim, Y. J.; Kim, K. S.; Ozyilmaz, B.; Ahn, J. H.; Hong, B. H.; Iijima, S. *Nat. Nanotechnol.* **2010**, *5*, 574–578.
(11) Park, J. U.; Nam, S. W.; Lee, M. S.; Lieber, C. M. *Nat. Mater.* **2012**, *11*, 120–125.
(12) Zhu, Y.; Murali, S.; Stoller, M. D.; Ganesh, K. J.; Cai, W.; Ferreira, P. J.; Pirkle, A.; Wallace, R. M.; Cychosz, K. A.; Thommes, M.; Su, D.; Stach, E. A.; Ruoff, R. S. *Science* **2011**, *332*, 1537–1541.
(13) An, X.; Simmons, T.; Shah, R.; Wolfe, C.; Lewis, K. M.; Washington, M.; Nayak, S. K.; Talapatra, S.; Kar, S. *Nano Lett.* **2010**, *10*, 4295–4301.
(14) An, X.; Bulter, T. W.; Washington, M.; Nayak, S. K.; Kar, S. *ACS Nano* **2011**, *5*, 1003–1011.
(15) Li, X.; Zhu, H.; Wang, K.; Cao, A.; Wei, J.; Li, C.; Jia, Y.; Li, Z.; Li, X.; Wu, D. *Adv. Mater. (Weinheim, Ger.)* **2010**, *22*, 2743–2748.
(16) Wintterlin, J.; Bocquet, M. L. *Surf. Sci.* **2009**, *603*, 1841–1852.
(17) Li, X.; Cai, W.; Colombo, L.; Ruoff, R. S. *Nano Lett.* **2009**, *9*, 4268–4272.
(18) Li, X.; Magnuson, C. W.; Venugopal, A.; An, J.; Suk, J. W.; Han, B.; Borysiak, M.; Cai, W.; Velamakanni, A.; Zhu, Y.; Fu, L.; Vogel, E. M.; Voelkl, E.; Colombo, L.; Ruoff, R. S. *Nano Lett.* **2010**, *10*, 4328–4334.
(19) Gao, L.; Guest, J. R.; Guisinger, N. P. *Nano Lett.* **2010**, *10*, 3512–3516.
(20) Loginova, E.; Bartelt, N. C.; Feibelman, P. J.; McCarty, K. F. *New J. Phys.* **2008**, *10*, 093026.
(21) Loginova, E.; Bartelt, N. C.; Feibelman, P. J.; McCarty, K. F. *New J. Phys.* **2009**, *11*, 063046.
(22) Gruneis, A.; Kummer, K.; Vyalikh, D. V. *New J. Phys.* **2009**, *11*, 073050.
(23) Fan, L.; Li, Z.; Xu, Z.; Wang, K.; Wei, J. *AIP Adv.* **2011**, *1*, 032145.
(24) Wofford, J. M.; Nie, S.; McCarty, K. F.; Bartelt, N. C.; Dubon, O. D. *Nano Lett.* **2010**, *10*, 4890–4896.
(25) Barnard, A. S.; Snook, I. K. *Model. Simul. Mater. Sci. Eng.* **2011**, *19*, 054001.
(26) Saadi, S.; Pedersen, F. A.; Helveg, S.; Sehested, J.; Hinnermann, B.; Appel, C. C.; Norskov, J. K. *J. Phys. Chem. C* **2010**, *114*, 11221–11227.

(27) Gao, J.; Yip, J.; Zhao, J.; Yakobson, B. I.; Ding, F. *J. Am. Chem. Soc.* **2011**, *133*, 5009−5015.
(28) Gan, C. K.; Srolovita, D. J. *Phys. Rev. B* **2010**, *81*, 125445.
(29) Zangwill, A.; Vvednsky, D. D. *Nano Lett.* **2011**, *11*, 2092−2095.
(30) Chen, H.; Zhu, W.; Zhang, Z. *Phys. Rev. Lett.* **2010**, *104*, 186101.
(31) Miyaura, N.; Yanagi, T.; Suzuki, A. *Synth. Commun.* **1981**, *11*, 513−519.
(32) Kuntyi, O. I.; Stakhira, P. Y.; Cherpak, V. V.; Bilan, O. I.; Okhremchuk, Y. V.; Voznyak, L. Y.; Kostiv, N. V.; Kulyk, B. Y.; Hotra, Z. Y. *Micro Nano Lett.* **2011**, *6*, 592−595.
(33) Rushforth, R. *Platinum Met. Rev.* **2004**, *48*, 30−31.
(34) Favier, F.; Walter, E. C.; Zach, M. P.; Benter, T.; Penner, R. M. *Science* **2001**, *293*, 2227−2231.
(35) Kopinke, F. D.; Mackenzie, K.; Kohler, R. *Appl. Catal., B* **2003**, *44*, 15−24.
(36) Parambhath, V. B.; Nagar, R.; Sethupathi, K.; Ramaprabhu, S. *J. Phys. Chem. C* **2011**, *115*, 15679−15685.
(37) Huang, C. C.; Pu, N. W.; Wang, C. A.; Huang, J. C.; Sung, Y.; Ger, M. D. *Sep. Purif. Technol.* **2011**, *82*, 210−215.
(38) Vadahanambi, S.; Jung, J. H.; Oh, I. K. *Carbon* **2011**, *49*, 4449−4457.
(39) Hamilton, J. C.; Blakely, J. M. *Surf. Sci.* **1980**, *91*, 199−217.
(40) Bowker, M.; Morgan, C.; Perkins, N.; Holroyd, R.; Fourre, E.; Grillo, F.; MacDowall, A. *J. Phys. Chem. B* **2005**, *109*, 2377−2386.
(41) Yokoyama, H.; Numakura, H.; Koiwa, M. *Acta Mater.* **1998**, *46*, 2823−2830.
(42) Hamada, I.; Otani, M. *Phys. Rev. B* **2010**, *82*, 153412.
(43) Kwon, S. Y.; Ciobanu, C. V.; Petrova, V.; Shenoy, V. B.; Baren, J.; Gambin, V.; Petrov, I.; Kodambaka, S. *Nano Lett.* **2009**, *9*, 3985−3990.
(44) Murata, Y.; Starodub, E.; Kappes, B. B.; Ciobanu, C. V.; Bartelt, N. C.; McCarty, K. F.; Kodambaka, S. *Appl. Phys. Lett.* **2010**, *97*, 143114.
(45) Tersoff, J.; Phang, Y. H.; Zhang, Z.; Lagally, M. G. *Phys. Rev. Lett.* **1995**, *75*, 2730.
(46) Raouafi, F.; Barreteau, C.; Desjonquères, M. C.; Spanjaard, D. *Surf. Sci.* **2001**, *482*, 1413−1418.
(47) Erwin, S. C.; Himpsel, F. J. *Nat. Commun.* **2010**, *1*, No.58.
(48) Gambardella, P. *J. Phys.: Condens. Matter* **2003**, *15*, S2533−S2546.
(49) Malarda, L. M.; Pimenta, M. A.; Dresselhaus, G.; Dresselhaus, M. S. *Phys. Rep.* **2009**, *473*, 51−87.
(50) Dresselhaus, M. S.; Jorio, A.; Hofmann, M.; Dresselhaus, G.; Saito, R. *Nano Lett.* **2010**, *10*, 751−758.
(51) Li, Z. C.; Zhang, W. H.; Fan, X. D.; Wu, P.; Zeng, C. G.; Li, Z. Y.; Zhai, X. F.; Yang, J. L.; Huo, J. G. *J. Phys. Chem. C* **2012**, *116*, 10557−10562.